A MATLAB-based ray launching simulation tool for VLC applications

Rafael Zafrilla and Jose F. Monserrat
Institute of Telecommunications and Multimedia Applications (iTEAM)
Universitat Politècnica de València
8G Building - access D - Camino de Vera s/n - 46022 Valencia (Spain)
Corresponding author: razafmag@teleco.upv.es

ABSTRACT

In this article we present a simulation tool for Visible Light Communications. This tool is based on MATLAB and uses the principles of ray launching methods for its calculations. The simulation tool uses a single LED as a transmitter and a single photodiode (PD) as a receiver. It allows for the assessment of different LED and PD characteristics and positions while considering both direct rays and first-order reflected rays. Subsequent versions of this program will focus on the study of VLC communications in an outdoor environment.

Keywords: VLC, ray tracing, ray launching, photodiode, LED.

1.- INTRODUCTION

Visible light communications (VLC) are a subset of optical wireless communications (OWC) technologies. Whereas OWC refers in a generic way to the communication in which light is used to carry a signal, VLC employs visible light that occupies the spectrum from 380 nm to 750 nm corresponding to a frequency spectrum of 430 THz to 790 THz [1].

Visible light communications' origins can be traced back to the ancient signal fires, followed by the Alexander Graham Bell's photophone in 1880. However, it was the emergence of solid state light sources that triggered the development of this novel technology [2]. At the beginning of the 21st century, a first approach to these applications can be found in the Nakagawa Laboratories. This ground-breaking research used white LEDs and different modulation schemes to conclude that it is feasible to use LED lights for wireless optical communications [3].

VLC offers multiple advantages compared to other technologies such as radio frequency (RF). Amongst these advantages, the most important ones are the possibility to use non-licensed channels, high bandwidth and low power consumption.

On the other side, some challenges that need to be overcome include the interference with the ambient light sources, the interference between VLC devices and the integration of the VLC with the existing technologies [1].

Just like any telecommunications system, a VLC system mainly consists of a transmitter, that utilizes the visible light source as a signal transmitter, air as a transmission medium (whether indoor or outdoor), and the appropriate photodiode as a signal receiving component [4]. There are several possible technologies to constitute each subsystem.

1.1 Transmitter

One of the key aspects of VLC is that it supports illumination and communication simultaneously. LEDs (Light Emitting Diodes) are the most extended option for the transmitter. Over the last decades, the development of LEDs has led to the gradual replacement of the incandescent and fluorescence light sources with solid state LEDs. The latter offer a bigger reliability, lifespan and efficiency. In addition to this, LEDs are capable of switching to different light intensities very fast, thus allowing the encoding of data.

There are several ways to generate white light from an inherently monochromatic device such as a LED. The main methods are based on a monochromatic LED utilizing yellow phosphor or a trichromatic approach (such as red, green and blue LEDs). Several advantages and disadvantages are bound to each method. Therefore, the appropriate transmitter type is selected based on the channel model.

The VLC data rate is dependent on the LED's modulation bandwidth. Although VLC systems have been demonstrated with both options, monochrome and trichrome, in [5] and [6], there are significant differences between them. While phosphorus-based white LEDs are less complex and less expensive compared to the RGB LEDs, they offer a lower modulation bandwidth, caused by the slow response of the phosphors (for a typical commercial LED, a bandwidth of 2MHz for the white component, and 10MHz for the blue component have been measured [7]). On the other side, RGB LEDs offer higher modulation bandwidths (around 180 MHz on the setup in [6]) at the expense of a bigger complexity.

There are several options to overcome the bandwidth limitations. Different methods, or a combination of them, that help to improve the data transmission rates are:

1) Digital signal processing (DSP), as in [8] and [9], where it is shown that the usage of DSP techniques can significantly enhance the performance of the VLC by improving the resilience to noise.

2) High-order modulations, such as a combination of DMT, multi-level modulation (QAM) as in [10].

3) Transmitter and receiver equalizations, as seen in [11], where blue-filtering and a post-equalization circuit achieves a better response.

4) Parallel transmissions like Single-Input-Single-Output (SISO) or Multiple-Input-Multiple-Output (MIMO), as in [12], which uses a combination of MIMO and OFDM techniques.

1.2 Receiver

There are mainly two types of VLC receivers: photodetectors (PD) or imaging sensors.

A photodetector (PD) is a semiconductor device that converts the received light into current. Commercial photodetectors with good responsivity are, for example, the silicon photodiode (Si PIN-PD) and the silicon avalanche photodiode (Si APD). Regarding the bandwidth, there are many photodiodes with bandwidths over 200 MHz (wider than the VLC LED transmitter) [4]. In [13] and [14], an analysis of the characteristics and performance of the different types of photodiodes is done.

Imaging sensors are basically multiple photodetectors arranged in a matrix on an integrated circuit. Already in [15] a 2-dimentional image sensor is proposed as a receiver, to overcome the limitations of an APD in terms of field of view (FOV). Other experiments have been carried out even by using the camera sensor of a smartphone [16].

One advantage of the CMOS image sensor usage is, due to the massive number of pixels available, its ability to spatially separate sources, like noise sources from LED transmission sources [17]. A downside of the commercially available imaging sensors is the frame rate, around 40 frames per second [18]. Higher rates would require high-speed cameras (e.g. 1000 fps as in [19]), thus increasing also the cost of the equipment.

1.3 Outdoor optical channel

VLC applications can be classified into two categories: indoor and outdoor.The outdoor optical channel has some characteristics that need to be considered, when considering VLC on the outdoor environment. Although VLC systems are preferably based on line-of-sight (LOS) configurations, in outdoor conditions there are many external light noise sources such as sun light or road and streets lights that may deteriorate the transmitted signal, and both natural and artificial ambient lights could induce shot noise on the receiver side. In addition, propagation characteristics of VLC drastically change with the atmospheric

conditions, which will condition the use of different modulation techniques. The work in [20] presented a VLC system suitable for outdoor applications, which allows a low data rate communication link ranging up to 40 m using commercially available LEDs and [21] used LED-based headlamps for V2V communication, reaching a distance of 20 m at a data rate of 2 Mbps. An experimental characterization of a traffic light to vehicle VLC link performance was carried out in [22].

To conclude this introduction, it should be pointed out that with respect to visible light communications, the outdoor applications are less explored when compared to those indoors. This is due to the fact that i) the dual use of LEDs (light and data) is not always practicable outdoors, ii) the level of interference and noise is considerably higher, iii) the alignment of transmitter and receiver is more complicated with high mobility, and iv) there are other technologies that adapt better to the outdoor environment, among others [23].

However, due to the great potential of VLC for vehicle applications it is important to understand and try to overcome these limitations. Current challenges regarding VLC usage in vehicular communications are:

i. increasing robustness to noise,
ii. increasing the communication range,
iii. enhancing mobility,
iv. increasing data range and
v. developing parallel visible light communications [24].

Most of the current and past investigations available have focused on indoor communications. However, the potential impact of VLC in outdoor environments, especially for vehicular communications, requires the extension of available models used in indoor for the outdoor case. The first phase into this direction consists in establishing a valid model with one or more LEDs as transmitter and one photodiode as receiver.

In this paper a MATLAB simulation tool for VLC modeling is presented. First, we introduce the ray launching method, which is the basis of our application, the modeling of the transmitter and the receiver elements and we explain the mathematical model of the LED-based VLC communications and how these models are applied in our program. Then, we show a block diagram of the whole application together with a description of the various subroutines, input and output data and internal structures. Lastly, we present the results of our simulations with different configurations and compare them with measurements done by other authors.

2.- SIMULATION TOOL

In this section, our simulation tool to reproduce the communication between an LED and a photodetector is presented. This tool is developed in MATLAB. In the first part, we present the two ray models that exist and the one chosen for our program. Then, we explain how the various elements of the VLC system are modeled and the block diagram or the program.

The main difference between our method and other researches that focus on MATLAB-based simulation tools for VLC applications like [25] is that the purpose of our tool is not to obtain results based on the direct application of mathematical models, but to take them as a base and apply the ray launching principles.

2.1 Ray launching

With wavelengths smaller than the surrounding obstacles, electromagnetic waves can be approximated by rays, applying the laws of optics. Mechanisms of reflection, diffraction and scattering have to be considered [26].

Ray models are usually based on one of the two ray construction techniques called ray tracing and ray launching. Whereas in ray tracing methods the paths are found by tracing a straight line joining the transmitter to the receiver, or to their respective image and checking if the reflection point lies within the limits of the considered reflector, in the ray launching method, a large set of rays is

launched from the source in 3D directions. Each ray represents a beam around its direction and the whole set of beams covers the 4 steradians solid angle of the sphere without holes or overlapping [27]. This simulation tool is based on the ray launching technique.

The identification of which rays eventually reach the receiver (and are considered for the received power calculations) is carried out through line-plane intersection methods. The straightforward option would be to check if any point of the line defined by an originating point and a direction is also a point of the plane that forms the receiver. However, this method would require a bigger effort compared to the algorithm that is used.

In [28], Möller and Trumbore describe an efficient algorithm for determining whether a ray intersects a triangle. In [29], Lagae and Dutré follow a similar approach but using quadrilaterals instead of triangles, which is, at least, as fast as the method with triangles. Although at first it can appear more logical to follow the second approach due to the geometry of the objects used by the simulation tool, our algorithm uses a tailored version of the method described in [28].

2.2 Modeling of the elements

2.2.1 Transmitter

As mentioned in the previous section, our simulation tool is based on the ray launching method. For this reason, the emitting LED is modeled as a large set of rays with a common origin. This origin is the position of the LED. For our purpose, the rays will not be launched in all directions of a sphere as stated before (4 steradians). Due to the shape and the emission pattern of an LED, only a hemisphere will be considered.

According to [30], the emitted light from an LED is assumed to have a Lambertian emission pattern, in which the radiant intensity depends on the angle of irradiance. The radiant intensity can be thus modeled using a generalized Lambertian radiant intensity

$$R_o(\theta) = \frac{m+1}{2\pi}\cos^{\mathrm{m}}(\theta),$$

where θ is the irradiance angle and m is order of Lambertian emission, which can be calculated

$$m = -\frac{\ln 2}{\ln \cos \Phi_{1/2}},$$

being $\Phi_{(1/2)}$ the semiangle at half power of a LED.

In addition to $\Phi_{(1/2)}$, our simulation tool uses the total optical power of the LED, P_{total}, for the calculations.

Having the total optical power of the LED, and considering that the LED will be represented by a number of individual rays, each of them must have a power that adds up to the power of the LED. The sum of the powers for every ray that reaches the receiver would result in the total power of the LED.

2.2.2 Receiver

At this stage of development, the receiver is modeled simply by a plane. The only purpose of the modeled receiver is to determine how many of the emitted rays or their corresponding reflections reach the receiver. The coordinates of the central point, the dimensions (width and length) and the normal vector of the receiver plane are part of the configuration parameters.

Other aspects that have to be considered in general according to Komine in [30] are the area of the receiver, A, the distance from the transmitter to the receiver, D_d, the angle of incidence, ψ, the gain of an optical filter, $T_s(\psi)$ and the gain of an optical concentrator, $g(\psi)$. If the incidence angle is bigger than the receiver's field of vision (FOV), Ψ_c, then the received power for that incidence angle is 0.

2.2.3 Optical link

Summing this up, Komine states that the received power, P_r, is derived from the transmitted optical power, P_t, as follows:

$$P_r = H(0) \cdot P_t$$

where $H(0)$ is the channel DC gain of an optical link

$$H(0) = \begin{cases} \frac{(m+1)A_r}{2\pi D_d^2} \cos^m(\theta)\, T_s(\psi) g(\psi) \cos(\psi), & 0 \le \psi \le \Psi_c \\ 0 & \psi > \Psi_c \end{cases}.$$

For our simulator, we consider no gains at the moment so, $T_s(\psi)=1$ and $g(\psi)=1$. The area of the receiver, A_r, is also not important for our purpose, since our calculation of the received power is based on the count of incident rays and the sum of their corresponding optical powers. The distance from the transmitter to the receiver, D_d, is calculated by the triangle-ray intersection algorithms.

2.2.1 Direct and reflected rays

There is a significant difference between the way direct and reflected rays are handled.

For each direct ray that reaches the receiver ($0 \le \psi \le \Psi_c$), our simulation tool calculates its received power as

$$P_{rd}(\theta) = \frac{(m+1)}{2\pi D_d^2} \cos^m(\theta) \cos(\psi)\, P_t(\theta).$$

For reflected rays, other aspects like the reflection coefficient of the reflective surface, ρ, and the total distance traveled by the ray must be considered. Also, according to Komine in [15], it is acceptable to make the assumption that all reflectors are Lambertian, so the angles involved in the reflection should also be considered in the calculations [30]. In the following equation, α is the angle of irradiance to a reflective point and β is the angle of irradiance to the receiver

$$P_{rr}(\theta) = \frac{(m+1)}{2\pi^2 D_{d1}^2 D_{d2}^2} \rho \cos^m(\theta) \cos(\alpha) \cos(\beta) \cos(\psi)\, P_t(\theta).$$

At the end of the simulation we obtain the total received power as

$$P_r = \sum_{\forall\theta} P_{rd}(\theta) + \sum_{\forall\theta} P_{rr}(\theta).$$

2.3 Block diagram

In this section we describe the overall process of the simulation tool.

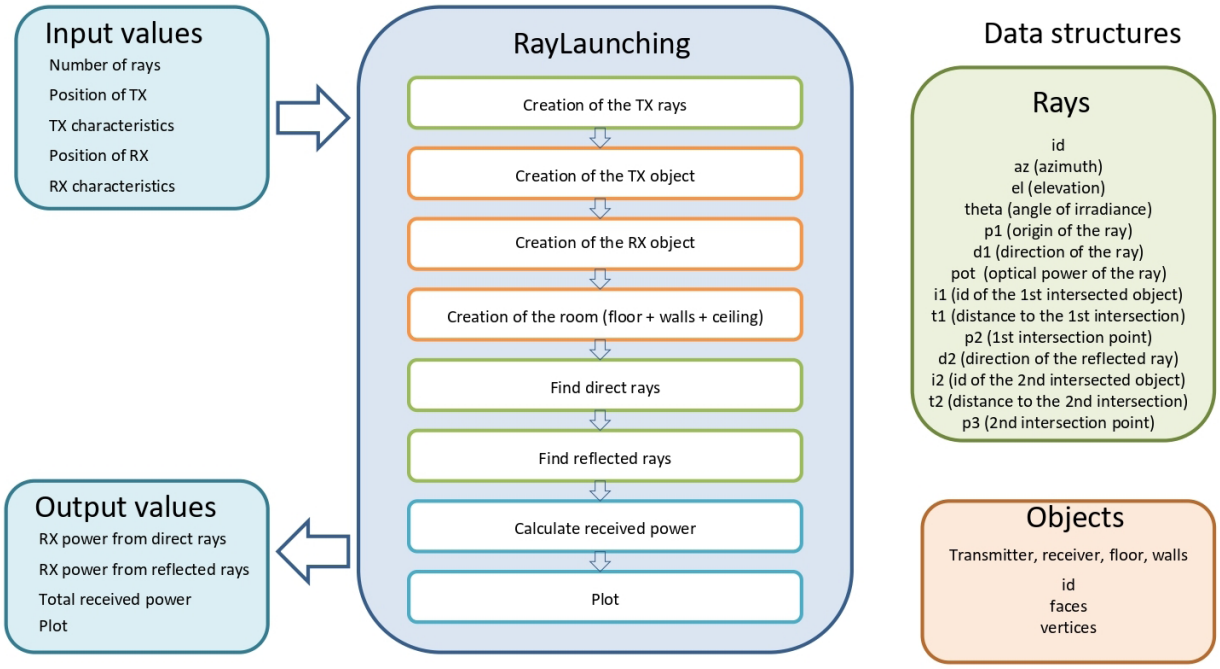

Figure 1: Block diagram of the simulation tool

On the left side of the figure we can see the input values that the program needs for the calculations:

- Number of rays: Configurable depending on the desired level of precision. This value determines how many rays will be launched.
- Position of TX: Cartesian coordinates of the position of the LED.
- TX characteristics: Values that describe the LED such as optical power and semiangle at half power.
- Position of RX: Cartesian coordinates of the position of the receiver plane (photodetector).
- RX characteristics: Values that describe the PD such as width, length and FOV.

The most important output values of the program are:

- RX power from direct rays: Total power received from the direct rays that reach the PD.
- RX power from reflected rays: Total power received from the reflected rays that reach the PD.
- Total received power: Sum of the two values mentioned above.
- Plot: A figure generated by MATLAB showing the scenario and the rays that reach the receiver.

On the right side of the picture we see the two structures that are used by the program: rays and objects. The rays structure contains all the data from the launched rays. The content of this structure is updated by several subroutines (depicted with a green border on the central part of the figure).

The objects structure contains the details of the different objects of the scenario: transmitter, receiver, walls and floor. Every object has a unique identifier and the list of faces and vertices (Cartesian coordinates) that form the object. This structure is updated by the subroutines depicted with an orange border on the central part of the figure.

The central part of the figure describes the different subroutines that are executed:

- Creation of the TX rays: This subroutine creates the set of rays that will be launched. All rays have a common origin given by the coordinates of the transmitter. The function that generates the rays does a linear spacing with the given "number of rays" value for the corresponding azimuth and elevation ranges. This ranges depend on the orientation of the LED. For instance, for a LED installed on the ceiling, azimuth $\in[0,2\pi]$, elevation: $\in[\pi,0]$. Then, each point of the mesh (currently in spherical coordinates) is converted to Cartesian coordinates. These points together with the center of the TX determine the direction of the ray. These values are stored in the rays structure.
- Creation of the TX object: An entry for the transmitter is stored in the objects structure.
- Creation of the RX object: With the given position, orientation, width and length of the receiver, the program generates the section of the plane that models the PD. This plane is split into two triangles and the corresponding coordinates of the vertices are stored in the objects structure.
- Creation of the room: Similar to the step above, given the position, orientation, width and length of the floor and walls, the program generates the corresponding planes and the vertices are stored in the objects structure.
- Find direct rays: Together with the following step, these two routines form the core of the program. For each ray in the rays structure, the triangle-ray intersection algorithm is run. The triangle-ray intersection function takes the ray origin and direction and returns the intersected object (i1), the intersection point (p2) and the distance from the origin of the ray to the intersection point (t1). These values are updated in the rays structure.

On this step the program calculates the corresponding received power of each ray, as described in section 2.2.4.

- Find reflected rays: For each ray in the rays structure that is not a direct ray (that means, that hasn't intersected with the receiver yet), the triangle-ray intersection algorithm is run.

Another loop runs through the rays structure and looks for the rays that have intersected a reflective surface (wall or floor). Given the intersection point and the direction of the ray, a function calculates the direction of the corresponding reflected ray. The program runs the triangle-ray intersection for this new ray and checks if it intersects the receiver. If that is the case, the intersection point (p3) and the distance from the origin of the reflected ray to the intersection point (t2) are updated in the rays structure.

The calculation of the corresponding received power, as described in section 2.2.4, is also done.

Calculate received power: For each received ray, the corresponding received power is added up and the received power (direct, reflected and total) is found.

- Plot: Finally, a plot with the transmitter, receiver, room and received rays (direct and reflected) is generated and shown.

3.- RESULTS AND DISCUSSION

In this section we present some results obtained with our simulation tool in order to prove the viability of using it for the simulation of real VLC scenarios.

We consider multipath environment in an empty room. The topology for the simulation is a cubic room (5 x 5 x 3 m) with plaster walls (ρ =0.83). The transmitter is a single LED source with $\Phi_{(1/2)}$=60° and P_{total}=1 W. The LED is located on the center of the ceiling (2.5, 2.5, 3). The receiver is a photodetector with FOV = 85° and area = 1 cm^2.

In order to validate that the simulation tool delivers correct results, a comparison between these results and calculations with the mathematical model is done. Two scenarios will be considered: a scenario where the photodetector is positioned right under the LED and a scenario where the PD is positioned in a different position. Simulations have been done with 250 000 launched rays.

As stated in section 2.2.4, the total power received by the PD is the sum of the contribution of the direct rays and the reflections in walls and other objects. In this case:

$$P_r = P_{rd} + P_{rr1} + P_{rr2} + P_{rr3} + P_{rr4},$$

where P_{rd} is the contribution of the direct rays and P_{rrk} is the contribution of the first-order reflections on each wall.

Scenario 1: Photodetector positioned right under the LED

In the first scenario, the photodetector is positioned right under the LED. That means, the PD is on the direction of maximum radiation of the LED. Due to the symmetry of the scenario, the individual contributions for the reflections on each wall will be the same.

Considering the direct rays' contribution and according to the mathematical model

$$P_{rd} = P_t \frac{(m+1)A_r}{2\pi D_d^2} \cos^{\mathrm{m}}(\theta)\cos(\psi) = 3.5368\ \mu W$$

where $P_t = 1\ W$, $m = -\frac{\ln 2}{\ln \cos 60} = 1$, $A_r = 1\ cm^2$, $D_d = 3\ m$, $\theta = 0$ and $\psi = 0$.

This contribution, according to the result of the simulation is 3.5359 μW.

Considering the reflected rays' contribution on any of the walls, according to the mathematical model

$$P_{rrk} = P_t \frac{(m+1)A_r}{2\pi^2 D_{d1}^2 D_{d2}^2} \rho \cos^{\mathrm{m}}(\theta)\cos(\alpha)\cos(\beta)\cos(\psi) = 0.022\ \mu W$$

where $P_t = 1\ W$, $m = -\frac{\ln 2}{\ln \cos 60} = 1$, $A_r = 1\ cm^2$, $\rho = 0.83$, $D_{d1} = 2.91\ m$, $D_{d2} = 2.91\ m$, $\theta = 59.03$, $\psi = 59.03$, $\alpha = 30.96$ and $\beta = 30.96$.

Due to the symmetry of the scenario, the total received power due to reflections is P_{rr}=0.089 μW. This contribution, according to the simulation is 0.0914 μW.

Table 1 shows the total received power in Scenario 1. From this outcome it can be seen that the results of the simulation are very close to the mathematical model. In addition, it is also evident that, in scenarios with Line-of-sight (LOS), the main contributors to the received power are the direct rays.

Table 1: Received power (direct and reflected) with the mathematical model and the simulation tool for Scenario 1.

	Model	Simulation
Direct rays	3.5368 μW	3.5359 μW
Reflected rays	0.089 μW	0.0914 μW
Total received power	3.6264 μW	3.6273 μW

Scenario 2: Photodetector positioned in a different position (0.5, 1, 0)

In the second scenario, the photodetector is positioned at a different position, in this case, at position (0.5, 1, 0), that is, away from the direction of maximum radiation of the LED. For the calculations, a similar approach as in the first scenario is followed, but considering that in this case there is no symmetry:

$$P_{rd} = P_t \frac{(m+1)A_r}{2\pi D_d^2} \cos^m(\theta)\cos(\psi) = 1.232\,\mu W$$

where $P_t = 1\,W$, $m = -\frac{\ln 2}{\ln \cos 60} = 1$, $A_r = 1\,cm^2$, $D_d = 3.905\,m$, $\theta = 39.80$ and $\psi = 39.80$.

This contribution, according to the result of the simulation is 1.2341 μW.

The reflected rays' contributions can be calculated with the mathematical model knowing the angles of irradiance, incidence and reflection. For the following calculations, these angles have been obtained also with the simulation tool. Table 2 shows the parameters that have been used for the calculations and also the received power from reflected rays, obtained both with the model and the simulation.

Table 2: Received power and parameter values used for the calculations of the reflected rays

	Left wall	Back wall	Right wall	Front wall
Reflection point	(0, 1.25, 0.50)	(1.73, 5, 1.84)	(5, 1.96, 1.93)	(1.07, 0, 0.86)
Irradiance angle, θ	48.18°	77.69°	67.27°	53.34°
Angles on the reflecting point, α, β	41.82°	12.31°	22.73°	36.66°
Incidence angle, ψ	48.18°	77.69°	67.27°	53.34°
Received power, P_{rrk} (model)	0.2613 μW	0.0021 μW	0.0056 μW	0.0728 μW
Received power (simulation)	0.2101 μW	0.0061 μW	0.0053 μW	0.0548 μW

Table 3 shows the total received power obtained with the model and the simulation. It can be seen that, again, the contribution of the reflected rays is much lower than the contribution of the direct rays. In addition, by comparing the total received power of the two scenarios it can also be seen that the power received in scenario 1 is higher than in scenario 2. This is due to the fact that the LED's direction of maximum radiation is normal to its surface, that is, right below it.

Table 3: Received power (direct and reflected) with the mathematical model and the simulation tool for Scenario 2.

	Model	Simulation
Direct rays	1.232 μW	1.234 μW
Reflected rays	0.342 μW	0.276 μW
Total received power	1.574 μW	1.510 μW

The following drawings show the plotted outcome of the ray launching for the two scenarios. Only rays that eventually reach the receiver are shown. The walls and the ceiling of the room have not been plotted for the sake of clarity.

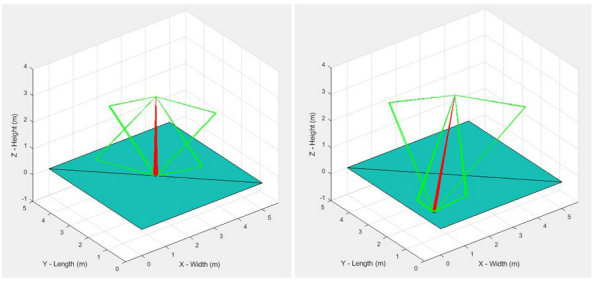

Figure 2: Results of the simulation. a) Photodetector positioned on the floor right under the LED (direction of maximum radiation) b) Photodetector positioned at a different position, in this case, at position (0.5, 1, 0)

To finalize this section, Figure 3 shows the received power distribution for the LOS path. As it can be seen, it has some symmetry and the peak power is observed at the center of the room (right below the LED). For this simulation, the receiver has been positioned in 1 024 different positions around the room. For each position, an individual simulation of the received power has been run. Lastly, the

total received power position (normalized) has been plotted.

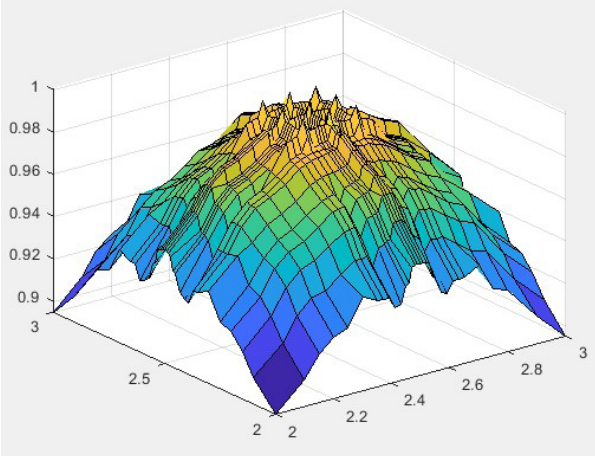

Figure 3: Spatial distribution of the received power (normalized)

4.- CONCLUSIONS

In this paper, we have reported the simulation program for visible light communication environment based on MATLAB. The program considers direct rays and first-order reflections at each wall. The results obtained by the simulations are accurate enough to conclude that this tool has a great potential in the study of VLC communications. Although the first results might indicate that the ray launching method is not as efficient as the mathematical models, it must be pointed out that the latter might face difficulties if the scenario gets more complex than a simple empty room. As the purpose of this tool is to be used for outdoor environments, which might not be easily covered by simple mathematical models, we think that it is worth continuing with this line of research.

However, to reach this purpose, some aspects need to be improved:

- Currently only a few part of the launched rays reaches the receiver. That means that most of the resources of the program are lost. The solution to this problem is to estimate which angle ranges (azimuth and elevation) should be used for the ray launching, so the most part of the launched rays reaches the receiver. This improvement is currently under development and will be included in next versions of the program.
- Although the results obtained with the simulation tool are close to the results of the mathematical model, it would be recommendable to calibrate the tool with real components. This leads us to the need for carrying out measurements in the lab, with a real hardware setup.
- The possibility to simulate MIMO configurations must be introduced, as it is a key aspect overcome the bandwidth limitations of the LED and increase the data transmission rate.

5.- REFERENCES

[1] L. U. Khan, "Visible light communication: Applications, architecture, standardization and research challenges," Digit. Commun. Networks, vol. 3, no. 2, pp. 78–88, 2017.

[2] S. Hranilovic, L. Lampe, S. Hosur, and R. Roberts, "Visible light communications: the road to standardization and commercialization (Part 2) [Guest Editorial]," IEEE Commun. Mag., vol. 52, no. 7, pp. 62–63, Jul. 2014.

[3] Y. Tanaka, T. Komine, S. Haruyama, and M. Nakagawa, "Indoor visible communication utilizing plural white LEDs as lighting," in 12th IEEE International Symposium on Personal, Indoor and Mobile Radio Communications. PIMRC 2001. Proceedings (Cat. No.01TH8598), p. F-81-F-85.

[4] C. Ghiu, "Visible Light Communication," in Advanced Trends in Wireless Communications, InTech, 2011.

[5] A. M. Khalid, G. Cossu, R. Corsini, P. Choudhury, and E. Ciaramella, "1-Gb/s Transmission Over a Phosphorescent White LED by Using Rate-Adaptive Discrete Multitone Modulation," IEEE Photonics J., vol. 4, no. 5, pp. 1465–1473, Oct. 2012.

[6] G. Cossu, A. M. Khalid, P. Choudhury, R. Corsini, and E. Ciaramella, "2.1 Gbit/s Visible Optical Wireless Transmission," in European Conference and Exhibition on Optical Communication, 2012, p. P4.16.

[7] D. C. O'Brien, L. Zeng, H. Le-Minh, G. Faulkner, J. W. Walewski, and S. Randel, "Visible light communications: Challenges and

possibilities," in 2008 IEEE 19th International Symposium on Personal, Indoor and Mobile Radio Communications, 2008, pp. 1–5.

[8] A. M. Cailean, B. Cagneau, L. Chassagne, V. Popa, and M. Dimian, "Design and performance evaluation of a DSP visible light communication receiver," in Proceedings of the 2014 IEEE 21st Symposium on Communications and Vehicular Technology in the BeNeLux, IEEE SCVT 2014, 2014, pp. 30–34.

[9] A.-M. Cailean, M. Dimian, V. Popa, L. Chassagne, and B. Cagneau, "Novel DSP Receiver Architecture for Multi-Channel Visible Light Communications in Automotive Applications," IEEE Sens. J., vol. 16, no. 10, pp. 3597–3602, May 2016.

[10] C. Kottke, J. Vučić, J. W. Walewski, K.-D. Langer, and S. Nerreter, "513 Mbit/s Visible Light Communications Link Based on DMT-Modulation of a White LED," J. Light. Technol. Vol. 28, Issue 24, pp. 3512-3518, vol. 28, no. 24, pp. 3512–3518, Dec. 2010.

[11] H. Li, X. Chen, B. Huang, D. Tang, and H. Chen, "High Bandwidth Visible Light Communications Based on a Post-Equalization Circuit," IEEE Photonics Technol. Lett., vol. 26, no. 2, pp. 119–122, Jan. 2014.

[12] Q. Wang, Z. Wang, and L. Dai, "Multiuser MIMO-OFDM for Visible Light Communications," IEEE Photonics J., vol. 7, no. 6, pp. 1–11, Dec. 2015.

[13] S. Fuada, A. P. Putra, and T. Adiono, "Analysis of Received Power Characteristics of Commercial Photodiodes in Indoor Los Channel Visible Light Communication Nonlinear Dynamic Modeling of a Fixed-Wing UAV View project High Speed Indoor Visible Light Communications View project Analysis of Rece," Artic. Int. J. Adv. Comput. Sci. Appl. Int. J. Adv. Comput. Sci. Appl., vol. 8, no. 7, 2017.

[14] P. Sharma and H. Sarangal, "Performance Comparison of APD and PIN Photodiodes using Different Modulation and Different Wavelengths," Int. J. Signal Process. Image Process. Pattern Recognit., vol. 9, no. 4, pp. 257–264, 2016.

[15] H. Binti Che Wook, T. Komine, S. Haruyama, and M. Nakagawa, "Visible light communication with LED-based traffic lights using 2-dimensional image sensor," in CCNC 2006. 2006 3rd IEEE Consumer Communications and Networking Conference, 2006., vol. 1, pp. 243–247.

[16] C. Danakis, M. Afgani, G. Povey, I. Underwood, and H. Haas, "Using a CMOS camera sensor for visible light communication," in 2012 IEEE Globecom Workshops, 2012, pp. 1244–1248.

[17] T. Yamazato et al., "Image-sensor-based visible light communication for automotive applications," IEEE Commun. Mag., vol. 52, no. 7, pp. 88–97, Jul. 2014.

[18] P. H. Pathak, X. Feng, P. Hu, and P. Mohapatra, "Visible Light Communication, Networking, and Sensing: A Survey, Potential and Challenges," IEEE Commun. Surv. Tutorials, vol. 17, no. 4, pp. 2047–2077, 2015.

[19] H. C. N. Premachandra et al., "High-speed-camera image processing based LED traffic light detection for road-to-vehicle visible light communication," in 2010 IEEE Intelligent Vehicles Symposium, 2010, pp. 793–798.

[20] N. Lourenco, D. Terra, N. Kumar, L. N. Alves, and R. L. Aguiar, "Visible Light Communication System for outdoor applications," in 2012 8th International Symposium on Communication Systems, Networks & Digital Signal Processing (CSNDSP), 2012, pp. 1–6.

[21] P. Luo, Z. Ghassemlooy, H. Le Minh, E. Bentley, A. Burton, and X. Tang, "Fundamental analysis of a car to car visible light communication system," in 2014 9th International Symposium on Communication Systems, Networks & Digital Sign (CSNDSP), 2014, pp. 1011–1016.

[22] K. Cui, G. Chen, Z. Xu, and R. D. Roberts, "Experimental characterization of traffic light to vehicle VLC link performance," in 2011 IEEE GLOBECOM Workshops (GC Wkshps), 2011, pp. 808–812.

[23] A. R. Ndjiongue and H. C. Ferreira, "An overview of outdoor visible light communications," Trans. Emerg. Telecommun. Technol., p. e3448, Jun. 2018.

[24] A. Cailean and M. Dimian, "Current Challenges for Visible Light Communications Usage in Vehicle Applications: A Survey," IEEE Commun. Surv. Tutorials, pp. 1–1, 2017.

[25] H. Q. Nguyen et al., "A MATLAB-based simulation program for indoor visible light communication system," in 2010 7th International Symposium on Communication Systems, Networks & Digital Signal Processing (CSNDSP 2010), 2010.

[26] B. E. Gschwendtner, G. Ww Olle, B. Burk, and F. M. Landstorfer, "RAY TRACING VS. RAY LAUNCHING IN 3{D MICROCELL MODELLING."

[27] J.-P. Rossi and Y. Gabillet, "A mixed ray launching/tracing method for full 3-D UHF propagation modeling and comparison with wide-band measurements," IEEE Trans. Antennas Propag., vol. 50, no. 4, pp. 517–523, Apr. 2002.

[28] T. Möller and B. Trumbore, "Fast, minimum storage ray/triangle intersection," in ACM SIGGRAPH 2005 Courses on - SIGGRAPH '05, 2005, p. 7.

[29] A. Lagae and P. Dutré, "An Efficient Ray-Quadrilateral Intersection Test," J. Graph. Tools, vol. 10, no. 4, pp. 23–32, Jan. 2005.

[30] T. Komine and M. Nakagawa, "Fundamental analysis for visible-light communication system using LED lights," IEEE Trans. Consum. Electron., vol. 50, no. 1, pp. 100–107, Feb. 2004.

6.- BIOGRAPHY

Rafael Zafrilla received his degree in Telecommunications engineering from the Universitat Politècnica de València (UPV) in 2013. Since then, he has developed his professional career in the field of mobile networks and GSM-R and he is a full-time maths high-school teacher. His research interests include optical wireless communications, free-space optics, and visible light communications.

Dr.-Ing. Jose F. Monserrat (H-index 23) received his MSc. degree with High Honors and Ph.D. degree in Telecommunications engineering from the Universitat Politècnica de València (UPV) in 2003 and 2007, respectively. He was the recipient of the First Regional Prize of Engineering Studies in 2003 for his outstanding student record receiving also the Best Thesis Prize from the UPV in 2008. In 2009 he was awarded with the best young researcher prize of Valencia. In 2016 he received the merit medal from the Spanish royal academy of engineering, in the young researcher category. He is currently full professor in the Communications Department of the UPV. His current research focuses on the design of future 5G wireless systems and their performance assessment. He has been involved in several European Projects, being especially significant his participation in NEWCOM, PROSIMOS, WINNER+, 5GXCAST and METIS/METIS-II where he led the simulation activities. He is currently Principal Investigator in two H2020 projects, 5G-CARMEN and 5G-SMART. He also participated in 2010 in one external evaluation group within ITU-R on the performance assessment of the candidates for the future family of standards IMT-Advanced. He co-edited two special issues in IEEE Communications Magazine on IMT-Advanced and 5G technologies and is co-editor of the Wiley book “Mobile and wireless communications for IMT-Advanced and beyond” and the Cambridge book “5G Mobile and Wireless Communications Technology”. Jose Monserrat is senior member of the IEEE, manages around 0.5 M€ yearly budget, holds 6 patents and has published more than 50 journal papers. Currently the group headed by Prof. Jose F. Monserrat consists of 3 Postdoctoral fellows, 8 PhD students and 2 Master students.